First Step in Multiscale Simulations of the Ionic Conductors: DFT Study of Oxygen Vacancy Migration Combined with Experimental Characterization of BSFC

Shruba Ganopadhyay,[1,2] Talgat Inerbaev,[1] Artëm E. Masunov,[1,2,3] Deanna Altilio,[4] Nina Orlovskaya,[4] Jaruwan Mesit,[5] Ratan Guha,[5] Ahmed Sleiti,[4] Jayanta Kapat[4],

[1]Nanoscience Technology Center, [2]Department of Chemistry, [3]Department of Physics, [4]Department of Mechanical, Materials, and Aerospace Engineering; [5]School of Electrical Engineering and Computer Science, University of Central Florida, 12424 Research Parkway, Suite 400, Orlando, Florida 32826 USA
amasunov@mail.ucf.edu

Abstract. Barium/Strontium Ferrate/Cobaltate (BSCF) was recently identified as a promising candidate for cathode material in intermediate temperature Solid Oxide Fuel Cells (SOFCs). We use plane wave pseudopotential Density Functional theory (DFT) to calculate the local ion distribution in this mixed perovskite, as well as activation energy barriers for oxygen vacancy migration. We found that cations are completely disordered, while oxygen vacancies exhibit a strong trend to from L-shaped trimers and square tetramers, Löwdin population analysis of the spin density indicates that the cobalt cations are in the intermediate spin state. Jahn-Teller distortion of the octahedral coordination around Cobalt cations, is observed both theoretically and experimentally and confirms its intermediate spin state. We optimize the structures of several transition states for oxygen anion moving into nearby oxygen vacancy site, surrounded by different cations. Theoretical activation energy for oxygen vacancy migration is found to be in good agreement with experimental data.

Keywords: Solid Oxide Fuel Cell, perovskite structure, mixed oxide, Density Functional theory.

1 Introduction

A Solid Oxide Fuel Cell is a device which converts chemical energy to electricity and consists solely of solid ceramic components. A single SOFC consists of an air electrode, electrolyte, and a fuel electrode. The function of the air electrode is to facilitate the reduction of oxygen molecules to oxide ions transporting electrons to the electrode/electrolyte interface and allowing gas diffusion to and from this interface. The function of the fuel electrode is to facilitate the oxidation of the fuel and the transport of electrons from the electrolyte to the fuel electrode interface. However, the detailed mechanism of oxygen reduction can be very complicated. According to a phenomenological description for the oxygen reduction reaction at the interface of porous cathode/electrolyte composite materials under SOFC operating conditions,

oxygen first adsorbs at the cathode surface with either an end- or a side-on intermediate. Then, the adsorbed oxygen species directly dissociates to monatomic oxygen ions (O^-) or is reduced to diatomic superoxo- and peroxo-like species (O^{2-} and O_2^{2-}, respectively), followed by dissociation to monatomic oxygen ions. Subsequently, the dissociated oxygen ions either reduce to O^{2-} followed by incorporation into the lattice or combine directly with an electron and an oxygen vacancy.[1] A better understanding of the structure and dynamics of the electrochemically active cathode surfaces and of electrocatalytic pathways involving coupled electron- and oxygen transfer processes is of paramount importance in predicting their electrochemical/catalytic performance for oxygen reduction and transport in SOFCs as well as selection of cathode for the SOFC.

BSCF referred as prominent material for intermediate temperature SOFC [2] and act as mix ionic electronic conductor (MIEC). [3] For this kind of materials cathode performance strongly depends on the rate of oxygen migration. Experimental studies to date are still unable to identify the active sites for the oxygen reduction reaction at the SOFC cathodes. Quantum chemical calculations may be a powerful approach to elucidate the O_2-cathode interactions as the technique can provide electronic structure, atomic structure, as well as the vacancy migration energetics of cathode materials. Till date all the calculation on vacancy migration energetics of BSCF was based on molecular dynamics simulation which is based on empirical parameters. [4] In this paper we predict the potential barriers for each type of oxygen site hopping based on first principle DFT simulation. The advantages of the first principle method over empirical method is the first one method requires no empirical input, and hence, does not suffer from some of the limitations inherent in the use of empirical potentials in molecular dynamics or atomistic Monte Carlo simulations.

In this paper we report results of micro-Raman spectroscopy study and Density Functional Theory calculations of structural and electronic properties of BSCF, including the spin states of B cations. The special attention is focused on oxygen vacancy ordering and activation energy for vacancy migration to clarify the stability and ionic conductivity of this material. Theoretical results are compared with experimental data.

2 Computational and Experimental Details

Our calculations are based on the DFT with the Perdew-Burke-Ernzerhof (PBE) exchange-correlation functional in the framework of Vanderbilt ultrasoft pseudopotentials[5] and plane wave basis set as it is implemented in Quantum-ESPRESSO program package.[6] The Brillouin-zone integrations were performed using Monkhorst-Pack grids using a 2×2×2 mesh for supercell calculations and. Spin polarized calculation with Marzari-Vanderbilt smearing [7] is used throughout. The geometry optimization was performed using Broyden-Fletcher-Goldfarb-Shanno algorithim. The wave function and electron density representation are limited by kinetic energies of 40 and 360 Rydberg respectively. We treated the Ba(5s,5p,6s), Sr(4s,4p,5s), Co(4s,3d), Fe(3d,4s) and O(2s,2p) electrons as valence states, while the

remaining electrons were kept frozen as core states. The accuracy of pseudopotentials was validated by computing the equilibrium lattice parameters (a) are compared with experimental value and bulk moduli (B) is also compared with available experimental value, and will be published elsewhere. For Co^{4+} we found intermediate spin state is the stable most among three possible spin states, low spin (LS), intermediate spin (IS), and high spin (HS) states (spin of S=1/2, S=3/2, and S=5/2); whereas for Fe^{4+} cations HS is the most stable among LS and HS states (S=1 and S=2).

For modeling the mixed perovskite material $Ba_{0.5}Sr_{0.5}Fe_{0.2}Co_{0.8}O_3$ we used a 2×2×2 supercell [2], containing 4 Ba atoms, 4 Sr atoms, 2 Fe atoms and 6 Co atoms, along with 24 Oxygen atoms (Fig. 1). This amounts to $Ba_{0.5}Sr_{0.5}Fe_{0.25}Co_{0.75}O_3$ formula unit, fairly close to experimentally observed stoichiometry. The numbers of the ions in the supercell, assigned in Fig. 1 are used in the following discussion.

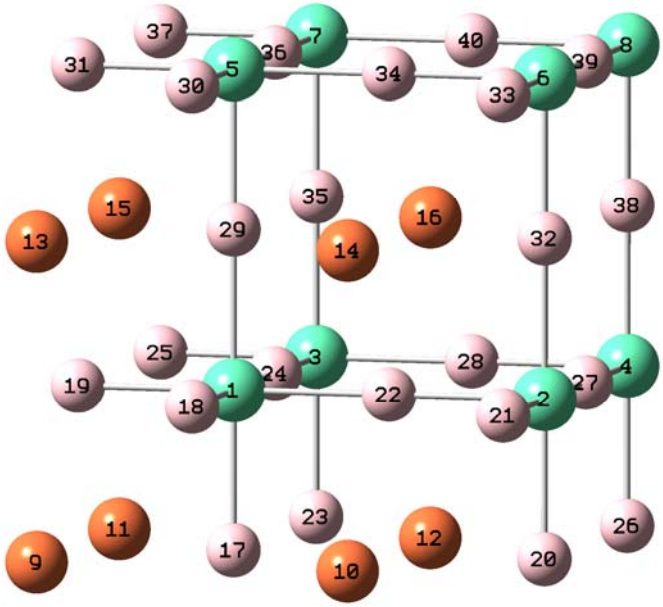

Fig. 1. ABO_3 perovskite supercell used for calculation. Here A is Barium or Strontium (marked by indexes 9-16), B is Iron or Cobalt (marked by indexs 1-8), and rest are Oxygen atoms (marked by indexes 17-40).

Activation energy was calculated for different ion distributions in supercell. Only ion hoping between symmetrically equivalent vacancy sites were considered. For each ion distribution, we perform two structural relaxation calculations: one for the stable supercell with one vacancy, and one transition state with oxygen ion in the middle of the XYX plane with OYZ angle of 45^0.

For all investigated configurations Boltzmann factor was calculated to estimate probability to observe this actual structure at SOFC operating temperature of 1150^0C. Micro-Raman spectroscopy was used to characterize the vibrational properties of BSCF perovskite. Renishaw InVia Raman microscope was used to study the

vibrational spectra of BSCF. The Raman microscope system comprises a laser (532 nm line of solid Si laser) to excite the sample, a single spectrograph fitted with holographic notch filters, and an optical microscope (a Leica microscope with a motorized XYZ stage) rigidly mounted and optically coupled to the spectrograph. The generated laser power was 25 mW. The average collection time for a single spectrum was 500s. The incident and scattered beams were focused with a long working distance 50x objective, which allowed keeping a laser spot as small as 2-3 μm. High temperature experiments were performed using a TMS600 heating stage (Linkam Scientific Instruments Ltd., UK) by heating/cooling of the samples to/from 600°C. The heating/cooling rate was 10^0C/min. Before BSCF measurements, the spectrometer was calibrated with a Si standard using a Si band position at 520.3 cm^{-1}. Renishaw Wire 2.0 software with a mixed Lorentzian and Gaussian peak fitting function was used to extract the peak's parameters.

3 Results and Discussion

3.1 Cation Spin States and Jahn-Teller Distortion

Löwdin population analysis in BSCF supercell is presented in the Table 1. It shows that the intermediate spin in Co and high spin states in Fe are most stable with the Boltzmann factor of 98%.

Table 1. Spin densitied on transition metal cations according to Lowdin population analysis for the different spin states of BSCF 2x2x2 superlattice, their relative energies and Boltzmann factoirs.

Multiplicity			Rescaled Lowdin spin-polarization		ΔE kcal/mol	Boltzmann factor (%)
Total	Fe^{+4} (d^4)	Co^{+4} (d^5)	Fe	Co		
23	2	3	3.61	2.59	9.66	2
27	4	3	3.62	3.12	0.00	98
35	2	5	4.31	4.16	35.23	0
39	4	5	4.6	4.58	101.37	0

After structural relaxation of BSCF supercell, we observed tetragonal Jahn-Teller distortion of the Co coordinatiton sphere (Fig. 2).

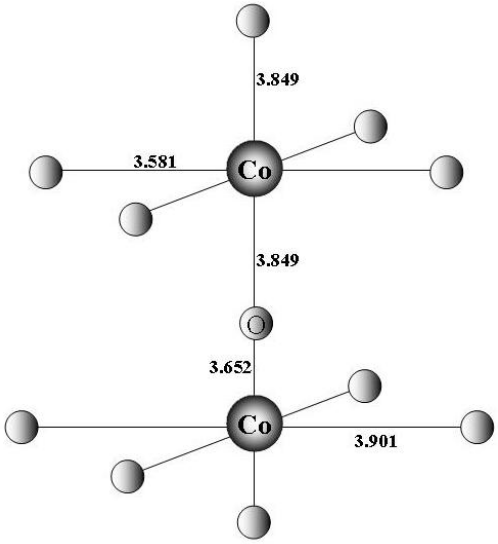

Fig. 2. Jahn-Teller distortion of coordination octahedron around of Co^{4+} cation is the evidence of intermediate spin state in BSCF supercell. Calculated equilibrium distances between Co^{4+} and nearest oxygen atoms are shown.

Since elongation and contraction both are observed in simultaneous fashion, overall symmetry of the cationic sublattice remains cubic. According to orbital splitting in octahedral crystal field, only the intermediate spin state of d^5-cation, such as Co^{+4}, is degenerate and subject to Jahn-Teller distortion. This theoretical evidence is confirmed by experimental Raman spectra, shown on Fig. 3.

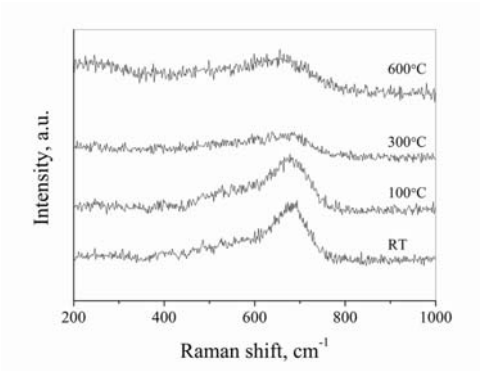

Fig. 3. Experimental Raman spectra of BSCF showing disappearance of ~675 cm^{-1} peak with elevated temperature.

In the ideal cubic perovskite structure all lattice sites have inversion symmetry. Therefore, first-order Raman scattering is forbidden and no Raman active band is expected to be found in cubic BSCF perovskite.[13] However, the broad asymptotic

band is detected at ~675 cm^{-1} as it is shown in Fig. 3. This broadband consists of the two overlapping bands which parameters such as peak positions and intensities could be detected using Full Width as Half Maximum approach. The appearance of these vibrations, forbidden in cubic structure, could be explained by the Jahn-Teller distortion in BSCF perovskite at room temperature. We assign these dynamic, local site distortion with the existence of the intermediate spin state Co^{4+} since it is a strong Jahn-Teller cation. [14] The rising temperature will relieve the Jahn-Teller distortion, the intensities of the bands are expected to decrease and the peaks become indistinguishable from the background. Therefore, the experimentally observed disappearance of two broad peaks at 600°C reflects the transition to a dynamically less distorted local structure of BSCF.

3.2 Cation disorder and vacancy clustering

For 2×2×2 supercell structure all 9 possible symmetrically inequivalent arrangements of Fe^{4+} and Co^{4+} cations at the B sites as well as Ba and Sr ion positions were taken into consideration. The results are presented in Table 2.

Table 2. Relative energies of BSCF supercells correcponding to different cation positions. The cation positions are labled according to Fig. 1, spin states of transition metals are S_{Fe}=2, and S_{Co} = 3/2. ΔE (kcal/mol) is the relative ground state energy measured in kcal /mol while C indicates the Boltzmann factors at 1150^0C.

Fe		Ba				ΔE kcal/mol	Boltzmann factor (%)
1	5	10	11	13	16	2.03	8
1	6	10	11	13	16	2.01	8
1	8	10	11	13	16	2.54	6
1	5	10	12	14	16	0.00	18
1	6	10	12	14	16	0.10	18
1	8	10	12	14	16	0.76	13
1	5	11	12	13	14	1.42	10
1	6	11	12	13	14	1.41	10
1	8	11	12	13	14	1.95	8

As one can see, all the cation distributions have similar relative stability and there is no preferred cation arrangement.

Next we calculate the relative stability of oxygen deficient supercell, with respect to the different vacancy positions. According to experimental data [10], the molar fraction of oxygen vacancies at 1150°C is δ=0.38. Therefore, we examined different structures with up to 4 oxygen vacancies per supercell. We removed one, two, three and four oxygen atoms from 2x2x2 supercell, which corresponds to stoichiometry of $Ba_{0.5}Sr_{0.5}Fe_{0.25}Co_{0.75}O_{3-\delta}$ (where δ = 0.125, 0.25, 0.375, 0.5). On the first step the simulation is performed for different ionic positions in stoichiometric (no defects) supercell. On the second step we remove one oxygen atom from the most stable

stoichiometric configuration and calculate relative energy of different multiplicities. The multiplicity with the lowest energy is used to optimize geometry of that particular configuration and Boltzmann factor is calculated to check the probability of the particular orientation. The same procedure is repeated for the oxygen vacant configurations. In order to determine the multiplicity of the stoichiometric supercell, one of two spin states for Fe^{+4} cation were combined with one of three spin states for Co^{+4} cation. From experiment, the $SrFe_{1-x}Co_xO_3$ compound is antiferromagnetic for $x<0.10$-0.15 and becomes ferromagnetic for $x\geq0.2$. Our calculations confirm these results [11]. We observe two vacancies in cis-position to the same Fe/Co ion (L-shape vacancy ordering) to be the most stable. This is in agreement with the experimental fact that the BSCF structure remains cubic in the observed oxygen deficiency range, while with similar compound with no Ba forms brownmillerite structure, where vacancy ordering is linear [12]. The relaxed geometry of BSCF with 2, 3, and 4 oxygen vacancies also changes the coordination of one, two, or four transition metal cations, adjacent to the vacancy, from ideal octahedron with two vertices missing to distorted tetrahedron (Fig. 4).

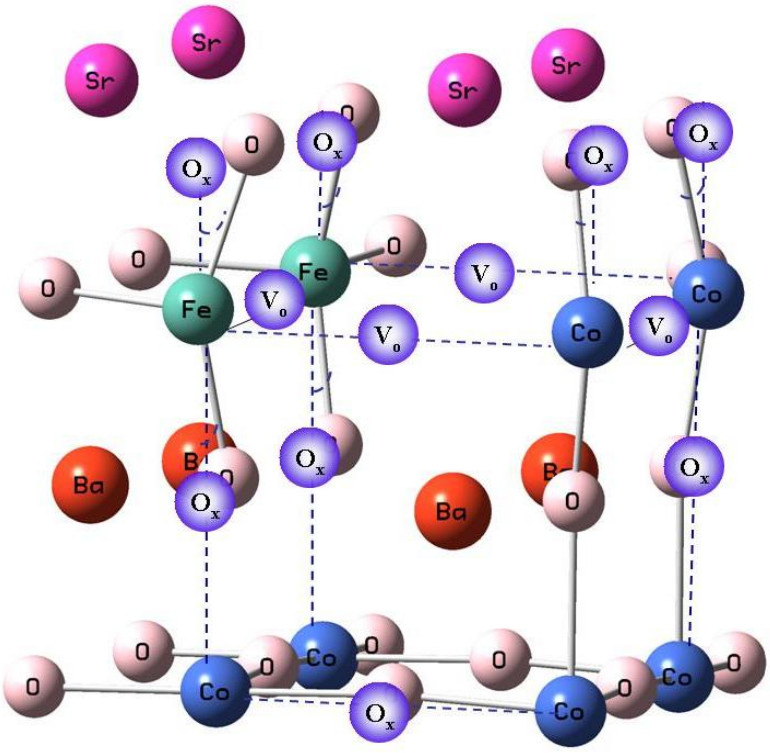

Fig. 4. $Ba_{0.5}Sr_{0.5}Co_{0.8}Fe_{0.2}O_{3-\delta}$ ($\delta = 0.5$) supercell ground state structure. Four oxygen vacancies are denoted as V_o. The positions of oxygen atoms in vacancy free lattice are labeled as O_x to demonstrate oxygen atoms displacement upon oxygen vacancies formation.

3.3 Activation energy for vacancy diffusion

Since our perovskite remains cubic throughout the fuel cell operation temperature range, we considered only cubic cross sections. According to Kilner [8] the oxygen vacancy can move by the following pathway described in Fig. 5. In this figure transition state is exactly the mid point, characterised by higher symmetry.

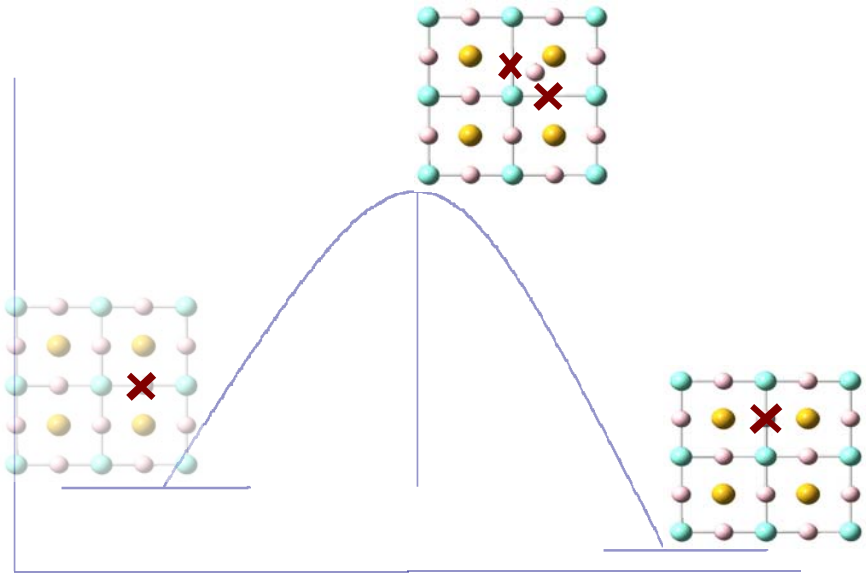

Fig. 5. Elementary step of Oxygen vacancy diffusion in a cubic perovskite

Previous molecular dynamics study for oxygen vacancy migration is done by Islam et. al. [9] also considered the pathway described in Fig. 5. In the previous section of this paper we conclude that in supercell cation orientation is random, so we considered various cation distributions in the supercell to calculate the activation energy. In order to calculate vacancy migration energy we took the difference between the ground state and the transition state. Since throughout the simulation we did not use any geometric constraint, the geometry and energetics of configuration with oxygen ion in the middle of the XYX plane and angle OYZ is 45^0 gives us proper transition state. On the other hand, first principles calculations are limited to relatively small

simulation cells. As a result, the barriers for oxygen hopping may be dependent on the specific distribution of dopant and catations in simulation cell. Because of the relatively large computational expense associated with the first principles calculations, we assume that the migration barriers for oxygen hopping are affected only by the two neighboring cations at the transition state. This assumption can be relaxed by mapping a large number of first principles calculations (for different local cation arrangements) and applying these results in kinetic Monte Carlo simulations. The kMC method has the advantage over molecular dynamics simulations (which are restricted to very short times) in properly sampling a large number of local environments in a statistically meaningful manner. However, in contrast to the molecular dynamics approach, this method assumes that oxygen diffusion is well represented by oxygen vacancy hopping through the edges of cation octahedral. The calculated activation energies are presented in Table 3. Our results are in good agreement with the experimental value for activation energy of oxygen ion migration is c.a. 10.5 kcal/mol.[10] Whereas the higher one shows a very stable ground state, which is less likely to go for vacancy migration.

Table 3 Activation energies of the oxygen vacancy hopping calculated for different cation arrangement in BSCF supercell. Fe and Ba cation positions are labeled according to the Fig. 1, the remaining positions are occupied by Co and Sr.

Fe		Ba				Vacancy		ΔE kcal/mol
1	8	10	11	13	16	22	24	-9.06
1	8	10	11	13	16	35	36	-7.83
3	5	10	12	14	16	35	35	-10.80
3	5	10	12	14	16	38	39	-9.86
1	8	10	12	14	16	35	36	-12.49
3	5	11	12	13	14	29	24	-8.27
3	5	11	12	13	14	38	39	-4.83

4 Conclusions

The present study demonstrates how plane wave DFT calculation can be used successfully to predict the electronic structure and oxygen transport property of doped perovskite BSCF. Our calculations predict the intermediate spin state and Jahn-Teller distortion for cobalt ions, both in agreement with experiment. The calculations show that the cations are completely disordered, while oxygen vacancies exhibit a strong trend to form cluster arrangements. We demonstrated that the most preferable position for oxygen vacancy in structure with $\delta = 0.125$ is between Fe and Co cations. The second vacancy has the most energy favorable position on site between Co cations. The preferential vacancy arrangements are predicted to be L-shaped for $\delta = 0.375$ and square for $\delta = 0.5$. This is in contrast with linear vacancy arrangement and phase transition to brownmillerite type of structure for similar material containing no Ba

ions. The activation energy of oxygen migration was found in the range of experimental data. The microscopic probabilities of oxygen migration, obtained in the present study can be used for the long timescale simulations with kinetic Monte-Carlo method. This work is currently under way.

5 Acknowledgements

This work is supported, in part, by NASA SFTI grant #NNCOGGA176 to UCF and NSF DMR project #0502765. The authors are grateful to DOE NERSC, I2lab and Institute for Simulation and Training (IST) and at University of Central Florida for the generous donation of computer time. TI is thankful to UCF NSTC and IST for additional support.

References

1. Choi Y., Mebane, D. S., Lin M. C., Liu, M.: Oxygen Reduction on $LaMnO_3$-Based Cathode Materials in Solid Oxide Fuel Cells. Chem. Mater. 19, 1690. (2007)
2. Shao, Z. P., Haile, S. M.: A high-performance cathode for the next generation of solid-oxide fuel cells, Nature 431, 170. (2004)
3. Shao, Z.P.: et al. Performance of a mixed-conducting ceramic membrane reactor with high oxygen permeability for methane conversion. J. Membr. Sci. 183, 181. (2001)
4. Fisher, C.A.J., et al.: Oxide ion diffusion in perovskite-structured $Ba_{1-x}Sr_xCo_{1-y}Fe_yO_{2.5}$: A molecular dynamics study. Solid State Ionics 177, 3425. (2007)
5. Vanderbilt, D.: Soft Self-Consistent Pseudopotentials in a Generalized Eigenvalue Formalism Physical Review B 41, 7892. (1990)
6. Baroni, S. et al.: Quantum-ESPRESSO. Available at http://www.pwscf.org (2006).
7. Marzari, N., Vanderbilt, D., Payne M. C.: Ensemble density-functional theory for ab initio molecular dynamics of metals and finite-temperature insulators. Physical Review Letters 79, 1337. (1997)
8. Kilner, J. A.: Fast Anion Transport in Solids. Solid State Ionics Solid 1983, 8, 201. (1997)
9. Islam, M. S.: Oxygen diffusion in $LaMnO_3$ and $LaCoO_3$ perovskite-type oxides Journal of Solid State Chemistry 124, 230. (1996)
10. Vanderbilt, D.: Soft Self-Consistent Pseudopotentials in a Generalized Eigenvalue Formalism. Physical Review B, 41, 7892 (1990).
11. Shein, I. R. et al.: Band structure and the magnetic and elastic properties of $SrFeO_3$ and LaFeO3 perovskites. Physics of the Solid State, 47: 2082 (2005).
12. McIntosh, S. J. et al.: Structure and oxygen stoichiometry of $SrCo_{0.8}Fe_{0.2}O_{3-\delta}$ and $Ba_{0.5}Sr_{0.5}Co_{0.8}Fe_{0.2}O_{3-\delta}$. Solid State Ionics, 177 1737 (2006).
13. Glazer, A. M.: Classification of Tilted Octahedra in Perovskites Acta Crystallographica - Structural Science B 28, 3384. (1972)
14. Orlovskaya, N. et. al.: Detection of temperature- and stress-induced modifications of $LaCoO_3$ by micro-Raman spectroscopy. Physical Review B (Condensed Matter and Materials Physics) , 72, 014122. (2005)